Vol. 42 (2011) ACTA PHYSICA POLONICA B No 3–4

RECENT RESULTS ON NEUTRON-RICH NUCLEI*

D. Bazin

National Superconducting Cyclotron Laboratory, Michigan State University
East Lansing, MI 48824-1321, USA

(Received February 7, 2011)

The study of the nuclear landscape on the neutron-rich side of the valley of stability has seen recent developments in the past few years at the NSCL. Progress has been made using a wide variety of methods and reaction probes, all based on the availability of fast radioactive beams produced via the projectile fragmentation technique. I will discuss the evolution of shell structure in neutron-rich nuclei located across the sd and fp shells, based on various results obtained, ranging from the discovery of the most neutron-rich nuclei in that region, to in-beam γ-ray spectroscopy using various reactions such as knockout of one or two nucleons, as well as inelastic scattering.

DOI:10.5506/APhysPolB.42.509
PACS numbers: 21.10.Dr, 25.60.Gc, 25.70.Mn, 29.38.Db

1. Introduction

Since the introduction in 1963 of the shell model as an independent-particle model to explain the structure of stable nuclei, and in particular the location of major shell gaps or so-called magic numbers, much progress has been made to understand the evolution of nuclear structure away from the valley of stability. The study of neutron-rich nuclei is particularly fruitful in this respect because they reach the farthest away from stable isotopes, and can therefore expose the most pronounced evolution of shell gaps. Already well known effects of this evolution are the appearance of intruder configurations and/or mixing in the ground state of neutron-rich nuclei, due to the variations of single-particle energies with neutron excess. A good example is the so-called island of inversion centered around ^{32}Mg, due to the shrinking of the $N = 20$ shell gap with decreasing proton number [1]. This and other effects of shell gap evolution are now being investigated with regards to first principles, using effective interactions where tensor components or the effect of 3-body forces are included [2,3].

* Presented at the Zakopane Conference on Nuclear Physics "Extremes of the Nuclear Landscape", August 30–September 5, 2010, Zakopane, Poland.

One of the recent achievements in this direction is the resolution of the so-called oxygen puzzle, in which the last bound neutron-rich isotopes of oxygen is ^{24}O, whereas fluorine isotopes have been observed up to ^{31}F so far. The fact that adding a single proton allows to bind 6 more neutrons in fluorine isotopes is puzzling, and has only been explained recently by the importance of 3-body forces [3]. Without the addition of 3-body forces in the interaction, ^{26}O and ^{28}O are predicted to be bound as the ground state energies continue to decrease at $N = 18$ and $N = 20$. The addition of 3-body effects in the interaction lead to a change of slope in the energies, which correctly predicts the drip-line at ^{26}O. It is quite remarkable that such a simple experimental fact like the existence or non-existence of a nucleus can have deep consequences on our understanding of nuclear forces. Moreover, these effects not included in the NN force appear to grow when going away from stability. The drip-line is, therefore, one of the best place to study this type of phenomenon.

The effects of shell evolution are widespread. As pointed out in the previous paragraph, they condition the limits of nuclear existence, via the mass or ground state energy of nuclei. As single-particle energies evolve, so does the gaps between orbitals, leading to the disappearance of shell gaps known for stable nuclei and the appearance of new ones. As orbitals get close to each other or even cross each other, mixed and intruder configurations arise in the wave functions. These also lead to deformation and the onset of collectivity. Among the many experimental tools available to study the effects of shell evolution, some are particularly well adapted to the use of fast radioactive beams such as those available at the NSCL. Three of these methods used for the study of neutron-rich isotopes at the NSCL are the search for new isotopes towards the neutron drip-line, in-beam γ-ray spectroscopy using various direct reactions, and finally the study of neutron-unbound states via invariant-mass spectroscopy.

2. Climbing towards the neutron drip-line

2.1. The search for ^{40}Mg

As illustrated in the introduction, locating the neutron drip-line experimentally can have great consequences on our understanding of nuclear binding. In an effort to push this exploration towards elements heavier than neon, an experiment aimed at the search for ^{40}Mg was conducted [4]. Located at $N = 28$, this nucleus was predicted to be bound by most mass models, including the most recent Finite Range liquid Drop Model (FRDM) [5] and Hartree–Fock–Bogoliugov (HFB-8) [6] calculations. Three background-free events were observed during the one week experiment, thanks to the use of a two-stage fragment separator scheme using the S800 beam line as a tagging section [4]. More surprising however was the observation of ^{42}Al, an odd–odd neutron-rich nucleus which in turn was predicted to be unbound by most mass models. Although only one ^{43}Al was recorded, it is very likely bound as well thanks to the added pairing energy of the two valence neutrons. Moreover, calculations show that the $1p_{3/2}$ orbital remains more or less constant as it is being filled, which means that ^{44}Al and ^{45}Al are probably bound as well. This makes reaching the drip-line in aluminum isotopes ever more challenging experimentally, and is also somewhat reminiscent of the oxygen situation: assuming ^{40}Mg is the last bound isotope of magnesium, adding a single proton to the $0d_{5/2}$ orbital could bring extra stability in the aluminum isotopes.

2.2. Changes in mass surface

The evolution of cross-sections of exotic nuclei produced via projectile fragmentation is very well reproduced by a systematics based on the relative binding energies of the fragments [7]. This observation supports the assumption that highly excited pre-fragments produced by fragmentation statistically populate the mass surface (abrasion–ablation model). Not only is this systematics useful to predict cross-sections of unobserved isotopes, but it can also provide insight into changes in the mass surface when plotted against the predictions of mass models.

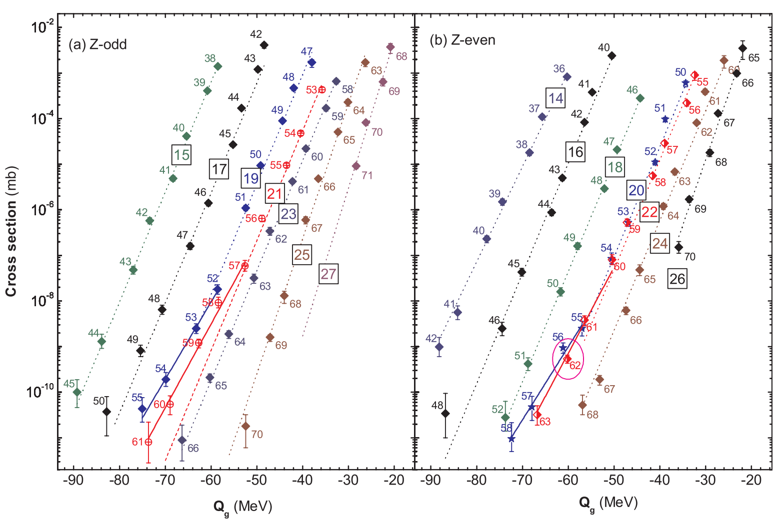

Fig. 1. Cross-sections plotted as a function of the mass difference between projectile and fragment (Q_g). The change in slope for neutron-rich isotopes of $19 \leq Z \leq 22$ indicates that these isotopes are significantly more bound than predicted by mass model used in the plot (from [8]).

Fig. 1 shows the Q_g systematics plot of neutron-rich isotopes with $15 \leq Z \leq 26$ produced via fragmentation of 130 MeV/u ^{76}Ge beam [8]. The masses used for the heaviest isotopes are taken from the KTUY [9] mass model. The change in slope for the most neutron-rich isotopes, most apparent between $Z = 19$ and $Z = 22$, indicates a deviation from this mass model, in turn an indication that more binding than predicted is observed in a region around ^{62}Ti. This region was predicted some time ago [10] as the location of a new island of inversion, where the closed shell structure found near stability vanishes, and ground states are taken by intruder states, leading to deformation and extra binding.

3. In-beam γ-ray spectroscopy

In-beam γ-ray spectroscopy is a powerful method especially well adapted to the study of rare isotopes produced via fast beam fragmentation, because of the high luminosity needed to compensate for the low production yields. In this method, the target nucleus becomes the probe since the rare isotopes can only be made as a beam, and the experiment is run in inverse kinematics. The high energy of the beams allows the use of thick targets and, at the same time, restricts the solid angle at which the projectile residue is emitted. A spectrometer placed at zero degree can then collect these residues with nearly 100% efficiency. The final state of the residue can be characterized from its emitted γ-rays, detected in an array surrounding the target, and Doppler-shifted back to the center-of-mass rest frame. This technique is now widely used at fragmentation facilities, and has produced considerable spectroscopic information in particular on the most neutron-rich isotopes within reach at those facilities.

3.1. Deformation in Cr isotopes

A relatively novel method to study collectivity in even–even neutron-rich isotopes uses inelastic scattering on a light (Be) target to populate excited states beyond the first 2^+ [11]. The isotopes ^{60,62,64}Cr have been studied using this method, and their first 2^+ and 4^+ excited states energies measured. Although unlike with a Coulomb excitation probe, the 2^+ cross-sections cannot readily be converted into transition strengths, they still convey qualitative information on the excitability — and therefore collectivity — of the nuclei, because the 2^+ state funnels the decay of other excited states. Fig. 2 (left) shows the relative 2^+ cross-sections of Cr and Fe isotopes for $N = 36$ to 40. The enhancement of the 2^+ cross-section in the Cr isotopes at $N = 40$ compared to the Fe isotopes indicates an onset of deformation in ^{64}Cr which is absent in its Fe isotone ^{66}Fe. This result seems to corroborate the mass surface evolution observed around ^{62}Ti in the Q_g systematics shown in Fig. 1.

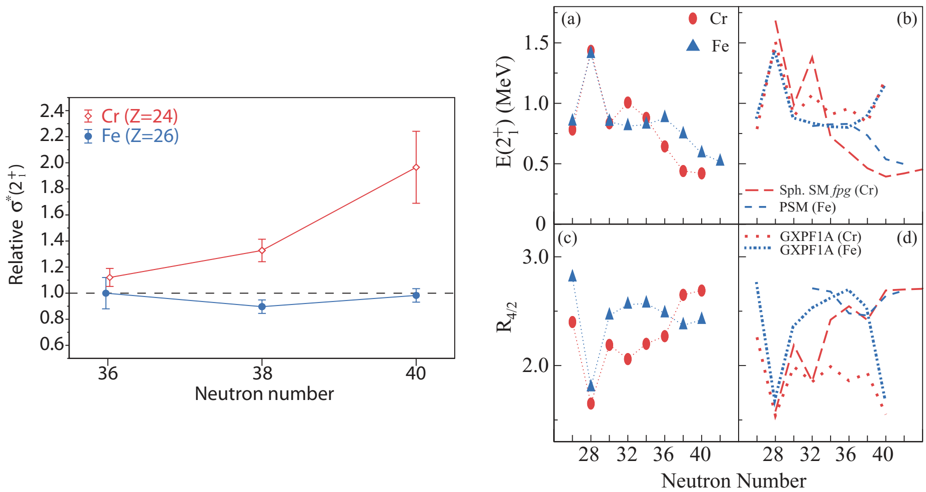

Fig. 2. Left: relative 2^+ cross-sections of neutron-rich Cr and Fe isotopes with $N = 36$ to 40. Right: 2^+ energies measured (a) and calculated (b), and 4^+ to 2^+ ratios $R_{4/2}$ measured (c) and calculated (d), for Cr and Fe isotopes. See text for details (from [11]).

Furthermore, shell model calculations using the GXPF1A interaction that does not include the $g_{9/2}$ orbital fail to reproduce the low 2^+ energies as well as the evolution of the $R_{4/2}$ ratios of the most neutron-rich Cr and Fe isotopes, as shown in Fig. 2 (right). The inclusion of the $g_{9/2}$ orbital in the projected shell model (PSM) using a deformed basis (for Fe isotopes), or in the spherical shell model using the fpg interaction (for Cr isotopes) on the other hand reproduces the data well. This indicates that significant contributions from the intruder $g_{9/2}$ orbital are present in the ground state wave functions of these isotopes when approaching $N = 40$. Note that this type of reaction is especially well adapted to the study of low-lying excited states, because the γ spectrum is essentially free of Bremsstrahlung radiation and low energy peaks can be identified even with low statistics.

3.2. Two-proton knockout spectroscopy

Another powerful method to study rare neutron-rich isotopes takes advantage of the difference in binding energy between valence protons and neutrons in such nuclei. The removal of two protons in a neutron-rich nucleus can only proceed as a single step reaction, because a two-step process would inevitably populate neutron-unbound states in the intermediate nucleus [12, 13]. The two-proton knockout cross-sections are therefore a good indicator of the overlap between the initial and final nucleus wave functions. This information is used in [14] to gain further insight in the structure evolution of the $N = 40$ isotones around the Cr–Ni region. Fig. 3 shows the cross-sections measured between the Ni, Fe and Cr isotopes at $N = 40$ and $N = 42$. The sudden drop by an order of magnitude between the ^{68}Ni to ^{66}Fe and the ^{66}Fe to ^{64}Cr cross-sections indicates a structural change at $N = 40$ between Fe and Cr, yet another clue adding to the previous observations exposed in the preceding sections. Similar conclusions on ^{60}Cr and ^{62}Cr are reached from a β-decay study of $^{60-63}$V isotopes [15].

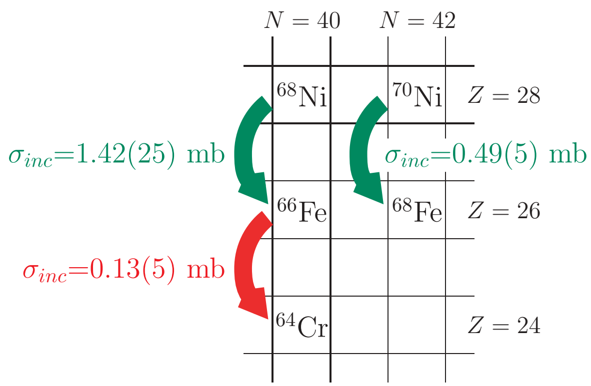

Fig. 3. Two-proton knockout cross-sections of $N = 40$ and $N = 42$ isotopes in the Cr–Ni region. The sudden drop between the Ni-to-Fe and Fe-to-Cr indicates a structural change between ^{66}Fe and ^{64}Cr (from [14]).

Another example of spectroscopy of a very neutron-rich nucleus using the two-proton knockout reaction method is the study of ^{36}Mg from the two-proton knockout of ^{38}Si [16]. In this experiment, a γ-ray is observed at 660 keV and assigned to the first 2^+ excited state in ^{36}Mg. Since the projectile ^{38}Si is well described by $0\hbar\omega$ shell model calculations, the two-proton partial cross-sections quantify the $0\hbar\omega$ components in final states of ^{36}Mg. After renormalization of the theoretical cross-sections by the observed two-nucleon suppression factor of $R_{\mathrm{S}}(2N) = 0.5(8)$ [13], a direct comparison of the partial cross-sections to the 0^+ ground state and first excited 2^+ state in ^{36}Mg can be carried out, as shown in Fig. 4. Neglecting possible feeding of the first excited 2^+ state from higher excited states in ^{36}Mg, the comparison shows good agreement with a large-scale Monte Carlo shell model calculation in which a large $2\hbar\omega$ component is present. This comparison shows that the low-lying states in ^{36}Mg are dominated by intruder configurations, which places this nucleus inside the island of inversion of the ^{32}Mg region.

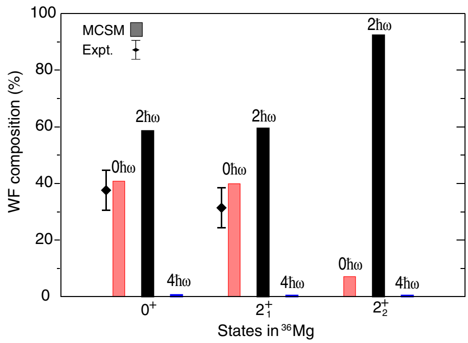

Fig. 4. Comparison of wave function composition between experiment and Monte Carlo shell model calculations. See text for details (from [16]).

Recent theoretical development have now shown that the parallel momentum distributions from two-nucleon knockout reactions can be used as a spectroscopy tool as well. Unlike one-nucleon knockout reaction parallel momentum distribution that can be used to identify the angular momentum of the removed nucleon [18], the two-nucleon knockout momentum distributions are sensitive to the spin and parity of the final state [17].

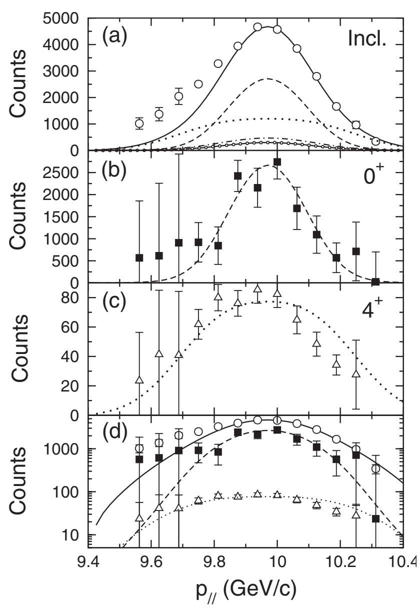

Fig. 5. Measured and calculated inclusive (a) and partial (b) and (c) parallel momentum distributions from the two-proton knockout of ^{38}Mg to final states in ^{26}Ne (from [17]).

The momentum distributions are calculated from an eikonal model using shell model two-nucleon amplitudes. So far only one comparison with experimental distributions has been performed on the the two-proton knockout from ^{28}Mg to ^{26}Ne final states. Fig. 5 shows this comparison for the 0^+ ground state (b) and first excited 4^+ state (c) in ^{26}Ne that have the largest cross-sections. Even though the statistics are still sparse (mostly due to the low γ-ray efficiency), the predictions agree well with the observed difference in shape of the momentum distributions. The prospects of using such comparisons to identify the final state reinforces the usefulness of this type of reaction for spectroscopy purposes.

3.3. Reactions involving neutron pick-up: ^{46}S and ^{48}Ar

Neutron drip-line exploration experiments have shown that fragments with an excess of neutrons compared to the projectile can still be produced with significant cross-sections at around 100 MeV/u. Taking advantage of this observation, the nuclei ^{46}S and ^{48}Ar were produced and studied using this type of reaction [19], starting from a ^{48}Ca primary beam as illustrated in Fig. 6 (left). The resulting 2^+ energies are compared to shell model calculations using the SDPF-NR interaction, and two of its modifications to try to match the observed data on Fig. 6 (right). The SDPF-NR2 modification is obtained by reducing the $2p2h$ core polarization contributions by interpolating between $Z = 20$ (original SDPF-NR) and $Z = 14$ for which the shell

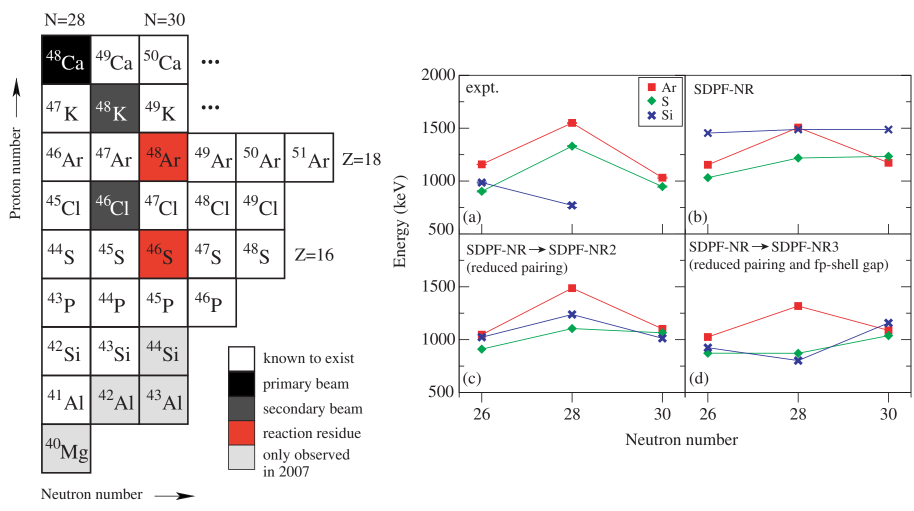

Fig. 6. Left: reactions involving neutron pick-up used to study the $N = 30$ isotopes ^{48}Ar and ^{46}S. Right: comparison of the 2^+ state energies with shell model calculations using the SDPF-NR interaction and two of its alterations (from [19]).

gap between $\pi d_{5/2}$ and $\pi f_{7/2}$ is larger. The SDPF-NR3 modification reduces the gap between the neutron $f_{7/2}$ and $p_{3/2}$, $p_{1/2}$ orbitals to get agreement with the Si isotopes. Neither modification can account for the evolution of the 2^+ states in all $Z = 14$, 16, 18 isotopes.

4. Neutron-unbound states spectroscopy

A large program of neutron-unbound state spectroscopy is ongoing at the NSCL, using the Modular Neutron Array (MoNA) [20] to detect fast neutrons around zero degree, and a dipole magnet to deflect the charged heavy residues into a detection system. The decay energy of the unbound state can be deduced from the momentum vectors of the neutron and heavy residue. Among the several results already obtained with this apparatus, the determination of the first 2^+ excited state in ^{24}O is certainly one of the prominent. The energy of the first 2^+ was measured at 4.72(11) MeV [21], a clear indication of a shell closure at $N = 16$ in ^{24}O. This relates directly to the observation of ^{24}O being the last bound oxygen isotope, as cited in the introduction, and illustrates the importance of the study of unbound states.

5. Conclusions

In this paper I have presented a small sample of the recent progress on neutron-rich nuclei at the NSCL. From these works and others, it is becoming clear that the shell structure observed initially in stable isotopes changes dramatically towards the neutron drip line. The neutron-rich side of the chart of nuclei is the ideal playground for mapping the shell structure evolution and ultimately understanding the underlying characteristics of the nuclear force that drives it, because the neutron potential goes asymptotically to zero towards the drip line. Not only new phenomena, such as neutron skins or haloes, have already been observed as a consequence, but also the large neutron excess that can be reached on this side of the stability line enables the exploration of the nuclear force on a vast isospin territory. For the same reason, it is also the most difficult region to reach. The future direction of the NSCL is precisely aimed at this reach, with the planned FRIB facility [22] slated to start operations in 2018. FRIB will be — among other things — a neutron-rich rare isotope factory, with several orders of magnitude larger yields than the present NSCL coupled-cyclotron facility.

REFERENCES

[1] V. Tripathi *et al.*, *Phys. Rev.* **C77**, 034310 (2008).
[2] T. Otsuka *et al.*, *Phys. Rev. Lett.* **104**, 012501 (2010).
[3] T. Otsuka *et al.*, *Phys. Rev. Lett.* **105**, 032501 (2010).
[4] T. Baumann *et al.*, *Nature* **449**, 1022 (2007).
[5] P. Möller *et al.*, *At. Data Nucl. Data Tables* **59**, 185 (1995).
[6] M. Samyn *et al.*, *Phys. Rev.* **C70**, 044309 (2004).
[7] O. Tarasov *et al.*, *Phys. Rev.* **C75**, 064613 (2007).
[8] O. Tarasov *et al.*, *Phys. Rev. Lett.* **102**, 142501 (2009).
[9] H. Koura *et al.*, *Prog. Theor. Phys.* **113**, 305 (2005).
[10] B.A. Brown, *Prog. Part. Nucl. Phys.* **47**, 517 (2001).
[11] A. Gade *et al.*, *Phys. Rev.* **C81**, 051304(R) (2010).
[12] D. Bazin *et al.*, *Phys. Rev. Lett.* **91**, 012501 (2003).
[13] J.A. Tostevin *et al.*, *Phys. Rev.* **C70**, 064602 (2004).
[14] P. Adrich *et al.*, *Phys. Rev.* **C77**, 054306 (2008).
[15] O. Sorlin *et al.*, *Eur. Phys. J.* **A16**, 55 (2003).
[16] A. Gade *et al.*, *Phys. Rev. Lett.* **99**, 072502 (2007).
[17] E.C. Simpson *et al.*, *Phys. Rev. Lett.* **102**, 132502 (2009).
[18] P.G. Hansen, J.A. Tostevin, *Annu. Rev. Nucl. Part. Sci.* **53**, 219 (2003).
[19] A. Gade *et al.*, *Phys. Rev. Lett.* **102**, 182502 (2009).
[20] T. Baumann *et al.*, *Nucl. Instrum. Methods* **A543**, 517 (2005).
[21] C.F. Hoffman *et al.*, *Phys. Lett.* **B672**, 17 (2009).
[22] `http://www.frib.msu.edu`